arXiv:1407.8255v1 [physics.ao-ph] 31 Jul 2014

The effect of surface buoyancy gradients on oceanic Rossby wave propagation

Xiao Xiao, K. Shafer Smith

Courant Institute of Mathematical Sciences, New York University, New York, NY

Shane R. Keating

School of Mathematics and Statistics, University of New South Wales, Sydney, NSW 2052, Australia

Abstract

Motivated by the discrepancy between satellite observations of coherent westward propagating surface features and Rossby wave theory, this paper revisits the planetary wave propagation problem, taking into account the effects of lateral buoyancy gradients at the ocean's surface. The standard theory for long baroclinic Rossby waves is based on an expansion of the quasigeostrophic stretching operator in normal modes, $\phi_n(z)$, satisfying a Neumann boundary condition at the surface, $\phi_n'(0) = 0$. Buoyancy gradients are, by thermal wind balance, proportional to the vertical derivative of the streamfunction, thus such modes are unable to represent ubiquitous lateral buoyancy gradients in the ocean's mixed layer.

Here, we re-derive the wave propagation problem in terms of an expansion in a recently-developed "surface-aware" (SA) basis that can account for buoyancy anomalies at the ocean's surface. The problem is studied in the context of an idealized Charney-like baroclinic wave problem set in an oceanic context, where a surface mean buoyancy gradient interacts with a constant interior potential vorticity gradient that results from both β and the curvature of the mean shear. The wave frequencies, growth rates and phases are systematically compared to those computed from a two-layer model, a truncated expansion in standard baroclinic modes and to a high-vertical resolution calculation that represents the true solution. The full solution generally shows faster wave propagation when lateral surface gradients are present. Moreover, the wave problem in the SA basis best captures the full solution, even with just a two or three modes.

Keywords: Rossby wave, surface buoyancy gradients, baroclinic instability, SQG

1. Introduction

Satellite altimetric observations show that wave speeds in the ocean are systematically greater than those predicted for linear first baroclinic Rossby waves (Chelton and Schlax, 1996). Several mechanisms have been suggest to explain these "too-fast" westward propagating surface signals: Doppler shifting and alteration of the PV gradient by the background mean flow (Killworth et al., 1997); topographic decoupling of upper-ocean waves (Tailleux and McWilliams, 2001); the combination of the two effects (Killworth and Blundell, 2003); conflating wave propagation with the westward propagation of coherent mesoscale eddies (Chelton et al., 2011; Early et al., 2011). Our aim here is neither to contradict nor promote the relevance of these approaches, but rather to point out the effect on surface signal propagation speeds of yet another nearly ubiquitous characteristic of the ocean: lateral gradients of surface buoyancy.

The possibility that surface gradients might significantly affect wave propagation is also suggested by their known effects on eddies. Eddy stirring against surface buoyancy gradients effectively generates ample

surface buoyancy anomalies, and a large number of recent studies indicate surface mesoscale and submesoscale structures consistent with the effects of such anomalies on quasigeostrophic dynamics (e.g. Xu and Fu, 2011; Ponte and Klein, 2013; Wang et al., 2013) . The limiting case of a flow entirely controlled by the surface buoyancy field is referred to as "surface quasigeostrophic" (SQG) theory. As an example for how surface gradients can affect wave propagation, consider the extreme case of vanishing interior potential vorticity (PV) gradients. The resulting Rossby edge wave has phase speed $\sim 1/\kappa$, where $\kappa^2 = k^2 + l^2$ and (k, l) is the two dimensional wavenumber. By contrast, the speed of a linear first baroclinic Rossby wave, derived by only assuming background interior PV gradients, is $\sim 1/\kappa^2$.

In most places, of course, the oceanic mean state exhibits both surface buoyancy and interior potential vorticity gradients; moreover, the mean state is almost always baroclinically unstable (Tulloch et al., 2011). Cases where instabilities are caused by interactions between surface shear flows and interior PV gradients are analogous to those of the classic atmospheric Charney instability problem (Pedlosky, 1987); following Smith (2007), we refer to these as "Charney type" instabilities. Fig. 1 shows an estimate of geographical regions that are Charney-unstable (see caption for details). In these regions, the existence of surface buoyancy gradients will change the nature of both the instability and the waves; and even in regions that are stable to Charney-type baroclinic instability, the surface buoyancy gradient may affect the wave propagation characteristics. Since it is difficult to separate propagation of a wave through the changing of mean state of the ocean from the production of baroclinically unstable waves from the mean state itself, we address this by focusing on the dispersion relation at small wavenumber, where the flow is stable or nearly stable.

Here we shall consider an idealized "ocean-Charney" problem, constructed by demanding the mean zonal velocity has a non-zero shear at the upper surface, zero shear at the lower surface, and a constant PV gradient in the interior; for example, with constant buoyancy frequency N, the resulting mean flow is quadratic in the vertical coordinate. [To add the effects of interior PV gradients, this can be augmented by the addition of a mean flow component proportional to the first baroclinic mode (a cosine in the case of constant N).] A numerical solution of the resulting eigenvalue problem for horizontal plane waves indeed shows that surface buoyancy gradients yield faster waves, relative to equivalent cases with no surface gradients (see Fig. 3; see caption and next section for details).

In addition to considering the physics of Rossby waves in the presence of surface buoyancy gradients, we also seek to find an efficient and transparent model for this process. Most of our theoretical understanding of wave and eddy dynamics in the ocean is based on models that have been simplified in the vertical: either by modal truncation or by using a small number of isopycnal layers. For example, Flierl (1978) studied the equivalence between layered models and continuous stratified flows and proposed a two-mode model that overcomes the inaccuracy due to the density step and upper-layer thickness of a layered model. Here we propose a model based on a truncated expansion in a set of surface aware (SA) modes recently developed by Smith and Vanneste (2013, SV13 hereafter). The SA modes represent surface-interior dynamics in a natural way, efficiently representing surface intensified motions, driven by surface buoyancy gradients, with just a few modes. The model is systematically compared to layered and standard modal truncations, and used to explore the effects of surface lateral buoyancy gradients on the dispersion relation.

The goals of this study are

1. to explore Rossby wave propagation on a background mean flow with surface buoyancy gradients, and
2. to introduce a new truncated model that efficiently captures the effect of surface buoyancy gradients on the wave problem.

The paper is organized as follows. Section 2 builds the linear ocean Charney plane wave problem and gives a brief review of the derivation of linear plane wave solutions for the quasigeostrophic (QG) equation. Full numerical solutions for the problem are computed and discussed. In section 3, we introduce the SA modes of SV13, and derive a wave model based on a truncated set of these modes. Section 4 presents analytic solutions for the case of constant stratification with certain mean flows, as well as numerical solutions for a broader range of flows. In addition, these solutions are compared to solutions of a two-standard-mode truncated model, as well as of the classic two-layer model. The efficiency of surface-aware modes is also discussed. Finally, section 5 concludes the paper.

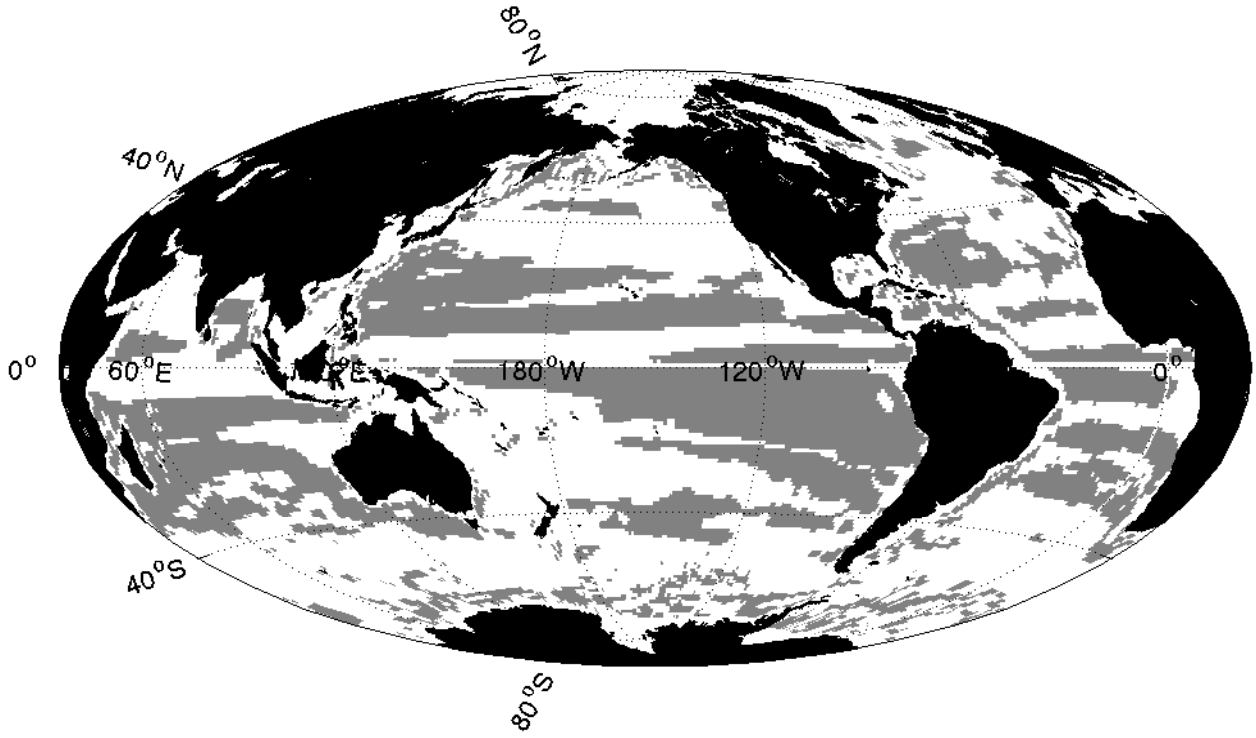

Fig. 1. Global maps of Charney instability (gray). OCCA (OCean Comprehensible Atlas) annal mean data is used (Forget, 2010). From the instability criteria, the ratio of dU/dz at ocean surface and the mean meridional PV gradient, Q_y, are computed and averaged over the top 500 meters. Charney type instability occurs when this ratio is negative, which is shown in gray.

2. A linear ocean Charney plane wave model

2.1. Construction of the background flow

We shall consider the quasigeostrophic (QG) plane wave problem linearized about an idealized zonal mean flow $U(z)$, with corresponding mean interior meridional PV gradient $Q_y(z)$ and mean meridional upper surface ($z = 0$) buoyancy gradient B_y given by

$$Q_y(z) = \beta - \frac{\mathrm{d}}{\mathrm{d}z}\left(\frac{f_0^2}{N^2}\frac{\mathrm{d}U}{\mathrm{d}z}\right) \quad \text{and} \quad B_y = -f_0\frac{\mathrm{d}U}{\mathrm{d}z}(0), \tag{1}$$

respectively, where f_0 is the mean Coriolis parameter, β is the meridional Coriolis gradient, and $N(z)$ is the buoyancy frequency. The lateral buoyancy gradient at the lower surface $z = -H$ is taken to vanish. The zonal background flows $U(z)$ are chosen to have the properties

$$\frac{\mathrm{d}U}{\mathrm{d}z}(0) = \Lambda^{\mathrm{dim}}, \quad \frac{\mathrm{d}U}{\mathrm{d}z}(-H) = 0, \quad \text{and} \quad \frac{1}{H}\int_{-H}^{0} U(z)\,\mathrm{d}z = 0,$$

where the superscript "dim" is added to distinguish the dimensional upper surface shear from a nondimensional version defined below. To proceed the velocity is written as a sum of two parts,

$$U(z) = U^S(z) + U^I(z),$$

where $U^S(z)$ is the "surface" part, with $\mathrm{d}U^S/\mathrm{d}z = \Lambda^{\mathrm{dim}}$ at $z = 0$ and vanishing lower surface shear, and $U^I(z)$ is the "interior" part, with vanishing shears at both the upper and lower surfaces. Ideally the interior PV gradient would be entirely controlled by the interior part of the mean shear, but the best we can do is demand the contribution of $U^S(z)$ to the PV gradient be a constant. The above constraints on the surface derivatives then imply

$$\frac{\mathrm{d}}{\mathrm{d}z}\left(\frac{f_0^2}{N^2}\frac{\mathrm{d}U^S}{\mathrm{d}z}\right) = \frac{f_0^2\Lambda^{\mathrm{dim}}}{HN_0^2}, \tag{2}$$

where $N_0 \equiv N(0)$.

A convenient choice for the interior part, satisfying the above constraints, is $U^I = U_1\Phi_1(z)$, where $\Phi_1(z)$ is the gravest non-constant eigenfunction (i.e. the first baroclinic mode) for the standard vertical mode problem

$$\frac{\mathrm{d}}{\mathrm{d}z}\left(\frac{f_0^2}{N^2}\frac{\mathrm{d}\Phi_j}{\mathrm{d}z}\right) = -\lambda_j^2\Phi_j, \quad \text{with} \quad \frac{\mathrm{d}\Phi_j}{\mathrm{d}z} = 0 \quad \text{at} \quad z = 0, -H, \tag{3}$$

and λ_j is the inverse Rossby radius for mode j. For reasons explained below, *we normalize* Φ_1 *such that its minimum value is -1.* The resulting composite flow $U(z)$ has thus an associated PV gradient consisting of a constant part plus a component proportional to the first baroclinic mode,

$$Q_y(z) = \beta - \frac{\Lambda^{\mathrm{dim}}f_0^2}{HN_0^2} + U_1\lambda_1^2\Phi_1(z). \tag{4}$$

Nondimensionalization

The parameters controlling the structure of the PV and surface buoyancy gradients are β, Λ^{dim} and U_1. To reduce the parameter space, and keeping in mind that we wish to compare results here to those of standard Rossby wave theory, we nondimensionalize lengths by the deformation scale $L_R \equiv N_0H/f_0$, and speeds by the long Rossby wave speed $U_R \equiv \beta L_R^2$. From here forward, all variables should be taken as nondimensional. The nondimensional surface buoyancy gradient is

$$\frac{B_y}{f_0U_R/H} = -\frac{f_0^2\Lambda^{\mathrm{dim}}}{\beta HN_0^2} \equiv -\Lambda$$

and the nondimensional interior PV gradient is then

$$\Pi(z) \equiv \frac{Q_y(z)}{\beta} = 1 - \Lambda + \xi\Phi_1(z) \quad \text{where} \quad \xi \equiv \frac{U_1\lambda_1^2}{\beta}.$$

Baroclinic instability in this flow is possible when either Λ has the opposite sign as Π for some z (Charney-type instability), or when Π itself changes sign (Phillips-type instability), or both. If $\Lambda = 0$, then by our choice of normalization that $\min(\Phi_1) = -1$, there will be a sign change in Π if $\xi > 1$, hence ξ is the supercriticality parameter for Phillips-type baroclinic instability. If $\xi = 0$ and $\Lambda \neq 0$, then Λ and $Q_y = 1-\Lambda$ must have the opposite sign, which will be true for $\Lambda < 0$ and $\Lambda > 1$ (thus the flow is stable only when $0 < \Lambda < 1$). When both parameters are nonzero, one can get stable flows, or instabilities of the Phillips, Charney or mixed type, with regime boundaries along the lines $\xi = \pm(1 - \Lambda)$.

Special Case I: Uniform background stratification

For constant background stratification $N(z) = N_0$, the nondimensional surface component of the mean velocity is

$$U^S(z) = \Lambda\left(\frac{z^2}{2} + z + \frac{1}{3}\right). \tag{5}$$

The first baroclinic mode with constant N is $\Phi_1(z) = \cos(\pi z/H)$, with $\lambda_1 = \pi/L_R$, thus the interior part has the form

$$U^I = \frac{\xi}{\pi^2}\cos(\pi z) \quad \text{with} \quad \xi = \frac{U_1\pi^2 f_0^2}{\beta H N_0^2}.$$

The top right panel of Fig. 2 shows U^S and the baroclinic modes $\Phi_j(z)$ are shown in the bottom left panel.

Special Case II: Nonuniform background stratification

As an idealization of the oceanic thermocline, we also consider

$$N^2 = N_0^2 e^{z/\delta}, \tag{6}$$

where $N_0^2 = N^2(0)$ and δ is the fractional scale depth. For this particular choice of the stratification profile, the non-dimensional surface velocity is, by equation (2),

$$U^S = \Lambda\delta\left[e^{z/\delta}(z + 1 - \delta) + 2\delta^2(1 - e^{-1/\delta}) - \delta\right]. \tag{7}$$

The interior flow U^I is proportional to the first standard baroclinic mode for the stratification (6), and ξ depends on its first eigenvalue. Both can be computed from a WKB approximation, but here we instead resort to a numerical solution. The surface part of the mean flow is plotted in the top right panel of Fig. 2, and the first baroclinic mode, $\Phi_1(z)$ — to which $U^I(z)$ is proportional — is shown in the bottom right panel.

2.2. Linear wave equations

For a plane wave solution $\psi(x, y, z, t) = \Re\{\psi_{kl}(z)\exp(kx + ly - \omega t)\}$ (and likewise for the PV and surface buoyancy), the QG equations linearized about $U(z)$ are (e.g. Vallis, 2006)

$$(U - c)b_{kl} - \Lambda\psi_{kl} = 0, \qquad z = 0, \tag{8a}$$

$$(U - c)q_{kl} + \Pi\psi_{kl} = 0, \qquad -1 < z < 0 \tag{8b}$$

where $c = \omega/k$ is the zonal phase speed, ω is the frequency, and $q_{kl}(z)$ and $b_{kl}(z)$ are the complex perturbation PV and surface buoyancy wave amplitudes at lateral wavenumber (k, l), respectively. The (nondimensional) PV and surface buoyancy amplitudes are related to the streamfunction amplitude $\psi_{kl}(z)$ by

$$q_{kl} = -\kappa^2\psi_{kl} + (s\psi'_{kl})', \quad \text{and} \quad b_{kl} = \psi'_{kl}(0) \tag{9}$$

where $\kappa^2 = k^2 + l^2$ and $s(z) = N_0^2/N^2(z)$, and the prime denotes a derivative in z. From here forward, except where confusion might ensue, the subscripts kl will be dropped.

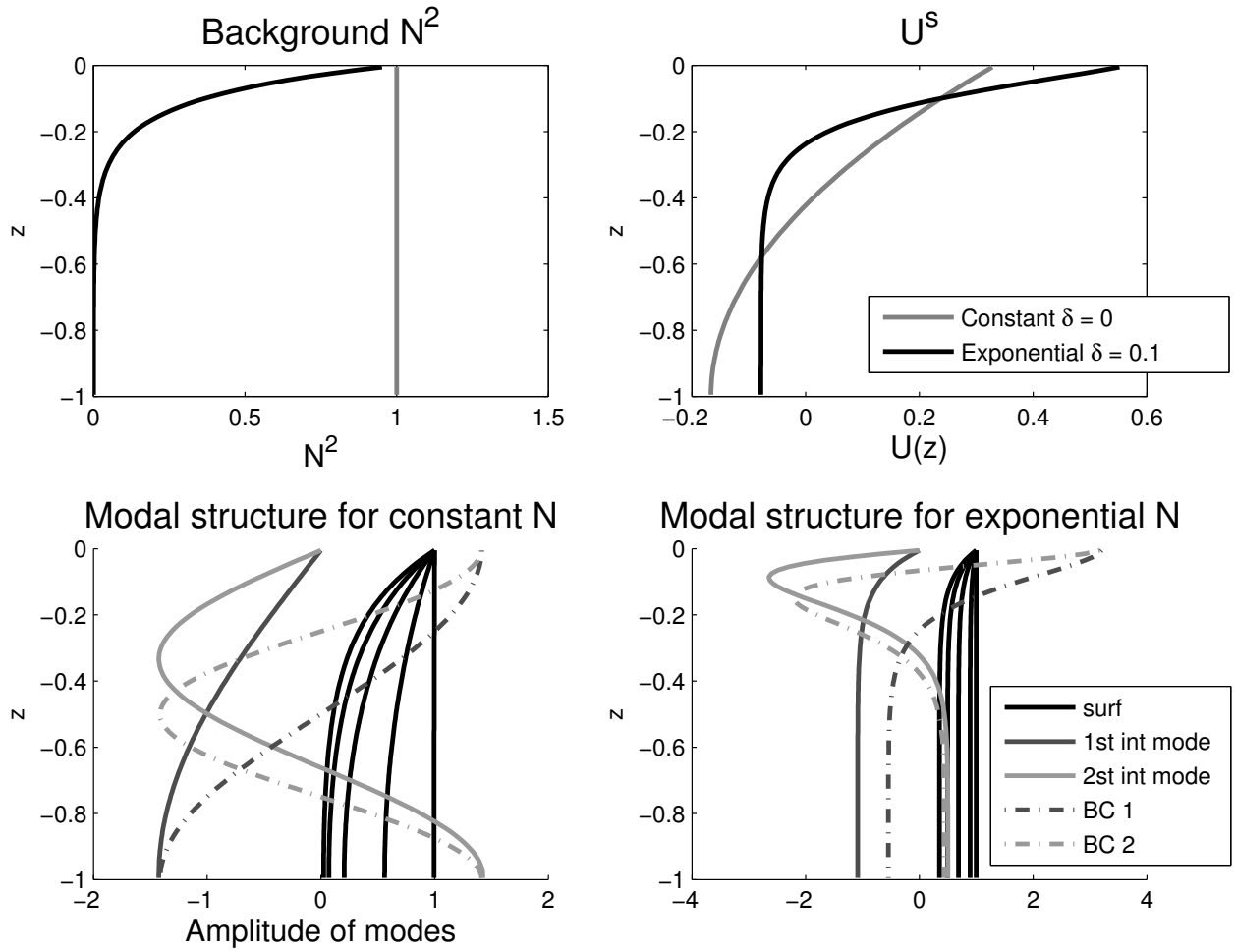

Fig. 2. Top left/right: Structure of background stratification and surface velocity, U^S, for constant/exponential stratification; Bottom left: Comparison of surface mode (from SA-mode basis) (solid) with barotropic (BT) mode (from standard normal modes basis) (dashed); Bottom right: Comparison of first two SA modes (solid) with first two standard modes (dashed).

2.3. Numerical solution to full wave problem

Before proceeding to the truncated solutions, we present numerical solutions of (9) for a range values of Λ and ξ, for the case $N = N_0$. In particular, we adopt a finite difference scheme with 100 equally spaced vertical layers, and solve the resulting linear eigenvalue problem using MATLAB. The baroclinic Rossby wave speed, denoted as c_+ hereafter, is the eigenvalue corresponding to the second gravest mode in the full calculation. Fig. 3 shows baroclinic wave speeds, at wavenumber $\kappa = 0.5$, as functions of Λ, for a range of ξ. According to our nondimensionalization, the baroclinic Rossby wave speed for a resting mean state ($\Lambda = \xi = 0$) is 1 (denoted by the dashed line). From the figure one can conclude that in most places the presence of a surface buoyancy gradient speeds up the wave: the magnitude of Rossby wave speeds will increase with increasing $|\Lambda|$. The sharp jumps near $\Lambda = 0$ occur when the type of the stability of the system changes or the system is only weakly unstable. For example, based on the instability criteria stated in the last paragraph, when $\xi < -1$, as Λ decreases from a large positive value, the system switches from a Charney instability with an eastward sheared surface velocity, to a mixed instability at $\xi = 1 - \Lambda$, then again to a Phillips instability when ξ crosses 0, and finally to a Charney instability (with westward sheared surface velocity) at $\xi \geq -1 + \Lambda$.

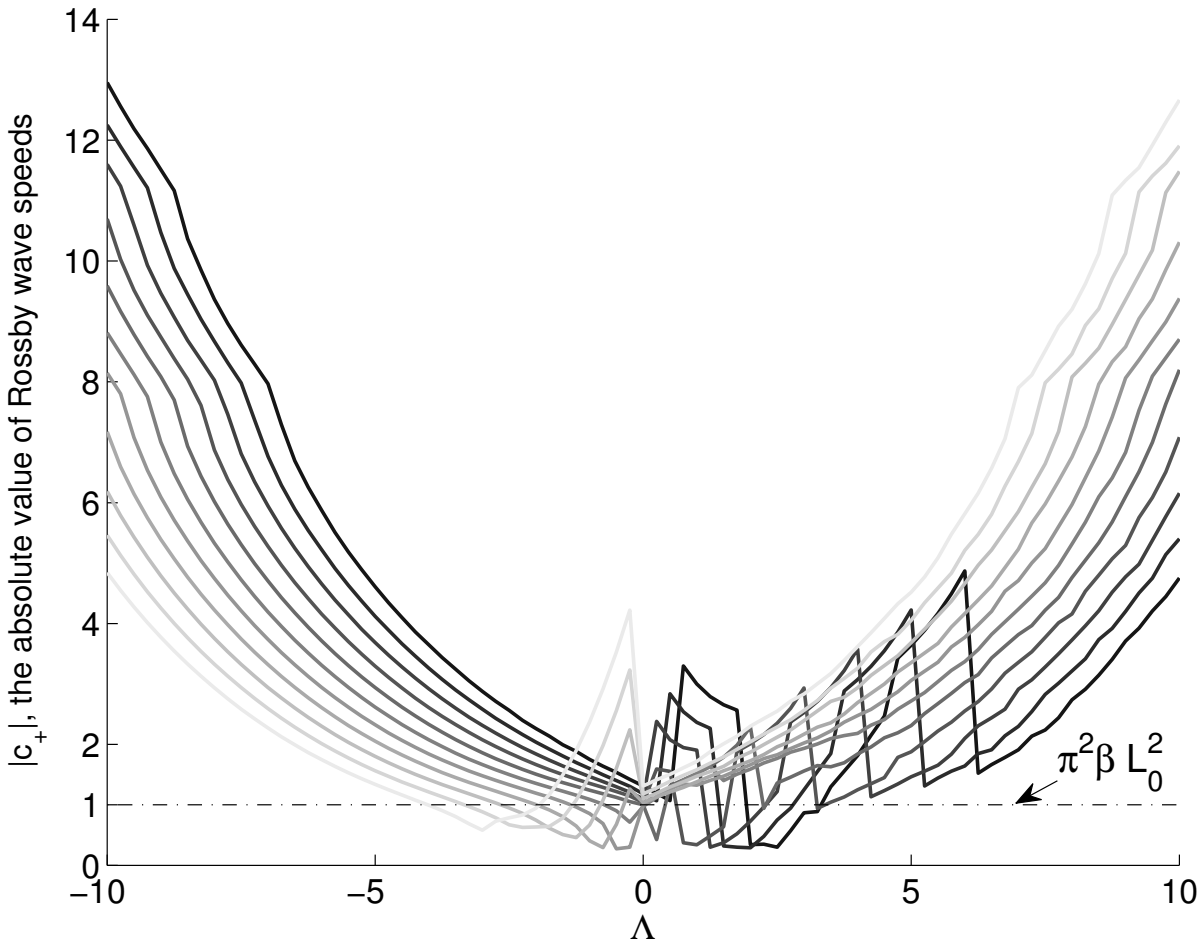

Fig. 3. Baroclinic Rossby wave speeds c_+ as a function of the upper surface buoyancy gradient $-\Lambda$ and the interior supercriticality ξ at wavenumber $\kappa = 0.5$ (twice the deformation scale). The values of ξ are integers varying from -5 (darkest) to 5 (lightest). Using OCCA data as in Fig. 1, and assuming $\beta = 2 \times 10^{-11}(\text{ms})^{-1}$, $f_0 = 10^{-4}$ s^{-1}, $N_0^2 = 4 \times 10^{-5}$ s^{-2}, and $H = 4000$ m, the nondimensional $|\Lambda| \lesssim 2$. In this nondimensionalization, the first baroclinic Rossby wave speed, $\beta(\pi L_D)^2$, is 1.

3. Modal projection on surface-aware modes

Having shown that surface gradients do tend to speed up baroclinic Rossby waves, we now attempt to capture this effect with a vertically truncated model. The new model will be compared to traditional truncations: a two-layer model and a two-standard-mode model.

We first consider a truncation of the dynamics projected onto the "surface-aware" (SA) modes of SV13. The reader is referred to that paper for full details, and a review, specialized to the present case with no buoyancy anomalies at the lower surface, is presented in Appendix A. Briefly, these modes are constructed to efficiently capture both surface and interior dynamics, while diagonalizing the energy. Nondimensional weights $\alpha_\pm$ control how sensitive the modes are to surface dynamics at the upper (+) and lower (−) surfaces, and in the limit $\alpha_\pm \to \infty$ (corresponding to vanishing buoyancy anomalies at both surfaces), the standard baroclinic modes are recovered. In the "ocean limit" considered here,$\alpha_- \to \infty$, and α_+ is suitably small (see below), consistent with a lower surface that has no significant buoyancy anomalies, but an upper surface that is dominated by them. In this limit, the gravest mode is a wavenumber-dependent evanescent mode akin to the vertical structure of an SQG solution; this mode becomes barotropic at very small wavenumber,

and replaces the standard barotropic mode. The higher modes are oscillatory, like the standard baroclinic modes, but shifted in phase.

Specifically, the SA streamfunction modes $\phi_j(z)$ in the ocean limit are solutions to the eigenvalue problem

$$(s\phi_0')' = \kappa^2\phi_0, \quad \text{with} \quad \phi_0'(0) = \frac{\mu_0^2}{\alpha_+}\phi_0(0), \quad \phi_0'(-1) = 0 \tag{10a}$$

$$(s\phi_j')' = -\lambda_j^2\phi_j, \quad \text{with} \quad \phi_j(0) = 0, \quad \phi_j'(-1) = 0, \quad j \geq 1 \tag{10b}$$

where $\mu_j^2 = \lambda_j^2 + \kappa^2$, and it is assumed that $\mu_0^2/\alpha_+ = O(1)$ and $\alpha_+ \ll 1$. As explained above, ϕ_0 is a wavenumber-dependent evanescent 'surface' mode and the rest are oscillatory 'interior' modes. In addition, the modes are orthogonal in the sense that

$$\int_{-1}^{0} s\phi_i'\phi_j' + \kappa^2\phi_i\phi_j \, \mathrm{d}z = \mu_j^2\delta_{ij}. \tag{11}$$

Note that other normalizations are possible (see SV13), but this one is most convenient for the analysis presented here. The traditional baroclinic modes (3) are recovered in the limit $\alpha_+ \to \infty$, and in this case ϕ_0 becomes the wavenumber-independent barotropic mode and the rest modes become baroclinic, i.e. the boundary conditions for all modes become $\phi_j'(0) = 0$.

For constant background stratification, the eigenvalue problem in (10) can be solved analytically with normalization (11), with solutions

$$\phi_0 = \frac{\sqrt{\alpha_+}}{\cosh\kappa}\cosh\left[\kappa(z+1)\right] \quad \text{and} \quad \phi_j = \sqrt{2}\sin\left[\left(j - \frac{1}{2}\right)\pi z\right] + O(\alpha_+) \tag{12}$$

for the surface and interior modes, respectively, with eigenvalues

$$\mu_0^2 = \alpha_+\kappa\tanh\kappa \quad \text{and} \quad \mu_j^2 = \kappa^2 + (j-1/2)^2\pi^2. \tag{13}$$

The structures of these ocean SA modes are shown in the bottom left panel of Fig. 2. Notice that, as with an SQG solution, the surface mode ϕ_0 is wavenumber-dependent but with different κ dependence than the SQG solution. The interior modes are sines instead of cosines, as the traditional baroclinic modes are, which represent interior motions with non-vanishing upper-surface derivatives. For the exponential stratification introduced in the previous section, these modes are also surface intensified and the structures are plotted in the bottom right panel of Fig. 2. In this case, the surface mode is nearly barotropic except near the surface, and the interior modes exhibit a similar structure to the traditional baroclinic modes, except for the Neumann boundary condition.

Projecting the streamfunction wave amplitude onto a finite set of ocean SA modes and using the orthogonality condition, the wave equation (9) can be posed as a discrete eigenvalue problem

$$c\mathbf{a} = \mathsf{B}\mathbf{a} \tag{14}$$

where $\mathbf{a} = \left(a_0, \ldots, a_n\right)^T$ is the coefficient vector and

$$\mathsf{B}_{ij} = \frac{1}{\mu_i^2}\left[\int_{-1}^{0}\left(\mu_j^2 U - \Pi\right)\phi_i\phi_j \, \mathrm{d}z + U(0)\phi_i(0)\phi_j'(0) - \Lambda\phi_i(0)\phi_j(0)\right] \tag{15}$$

The phase speeds c are the eigenvalues of the matrix B; the derivation of (14) and (15) are given in Appendix A.

4. Analytical and numerical solutions

In this section, we seek analytical and numerical solutions for the ocean Charney plane wave problem proposed in section 2 with the truncated SA mode model discussed in section 3. For cases with no interior

flow ($U^I = 0$), and either constant or exponential stratification, we approximate the solutions by using two-mode truncations in SA modes, and compare these to a two-mode truncation using traditional baroclinic modes, as well as to the wave speeds in a two-layer system. For the case when both exponential stratification and interior mean flow are present, we use a three-mode truncation for both modal bases to capture this more complicated dynamical structure.

4.1. Constant stratification, no 'interior' flow

Truncating the projected wave equation (14) to just two modes (i.e. $n = 1$) results in a 2×2 matrix equation that can be solved analytically if the integrals necessary to compute B in (15) can be computed in closed form. For constant stratification $N = N_0$ ($s = 1$), the ocean-limit SA modes and their eigenvalues are given in (12), and the necessary integrals can be found in terms of standard functions; details are given in Appendix B. For our purposes here, we additionally neglect the interior velocity, i.e. $\xi = 0$, so the interior mean PV gradient is $\Pi = 1 - \Lambda$. Since there can be no sign change of the interior PV gradient in this model, the only possible instability is of the Charney-type, which may occur when Λ and Π have opposite signs, e.g. when $\Lambda < 0$ or $\Lambda > 1$.

The details of the analytical solutions for the two-mode expansions in both the ocean limit SA modes and the traditional modes, as well as for the classic two-layer model, are relegated to Appendix B. Here we summarize just the small-κ Taylor-expansions of the baroclinic phase speeds for each of the three approximate solutions; they are

$$\text{SA modes:} \quad c_+ = -0.08 - 0.02\Lambda + \left(0.009 + 0.01\Lambda - 0.02\Lambda^2\right)\kappa^2 + O(\kappa^4), \tag{16a}$$

$$\text{Standard modes:} \quad c_+ = -0.025 + 0.13\Lambda + \left(0.01 - 0.01\Lambda + 0.02\frac{\Lambda^2}{1-\Lambda}\right)\kappa^2 + O(\kappa^2), \tag{16b}$$

$$\text{Two-layer:} \quad c_+ = -0.125 + \left(0.016 - 0.016\Lambda^2\right)\kappa^2 + O(\kappa^4), \tag{16c}$$

In the context of the standard baroclinic modal basis, c_+ is the first baroclinic wave speed. Comparing the small-κ approximations in (16), one can see that both modal truncated solutions depend on Λ at $O(1)$, while the two-layer approximation does not, thus the two-layer solution is not sensitive to changes of surface buoyancy gradient strength at large scale. Note also that in the standard-mode truncation (16b), there is a singularity at $\Lambda = 1$.

The upper panels of Fig. 4 plot the frequencies $\Re(\omega)$ and growth rates $\Im(\omega)$ for each truncated model (the analytical expressions are given in Appendix B), along side the full numerical solution discussed in section 2, as functions of wavenumber, for a few values of Λ. With a non-zero surface buoyancy gradient, the fact that the system generates faster westward Rossby wave speeds (negative values of $\Re(\omega)$) for small wavenumber is captured well by the SA modal solution. In addition, the growth rate from the SA modal solution is also very close to that in the full solution. The bottom panel of Fig. 4 shows the baroclinic wave speed for fixed wavenumber ($\kappa = 0.5$), as a function of Λ, for all three truncated models as well as for the full solution. In addition, the small-κ approximations in (16) for the three truncated models are shown as dashed lines. The full solution, plotted here as the lightest gray line, is the same as the curve on Fig. 3 with $\xi = 0$, but without the absolute value. The discontinuity of the full solution at $\Lambda = 1$ is because the system is stable when Λ is in between 0 and 1 and changes to eastward sheared Charney instability as Λ increases.

The results in Fig. 4 show that all solutions from the truncated models are close to the full solution when $\Lambda = 0$. In the cases where surface buoyancy gradients are present, the SA-mode truncation is closest to the true solution, in terms of both frequency and growth rate. The standard mode truncation, however, essentially fails to capture the dynamics. This may be because we have used the full velocity (instead of the projecting the velocity into modes first) in the wave equations (9); but when $\Lambda \neq 0$, the standard modes do not form a complete basis for U, resulting in grave errors. The two-layer approximation does somewhat better at large scales in the stable branch, while it completely underestimates both frequency and growth rate at larger wavenumbers. Moreover, the error of the layered model becomes larger in the next subsection when more complicated systems are considered.

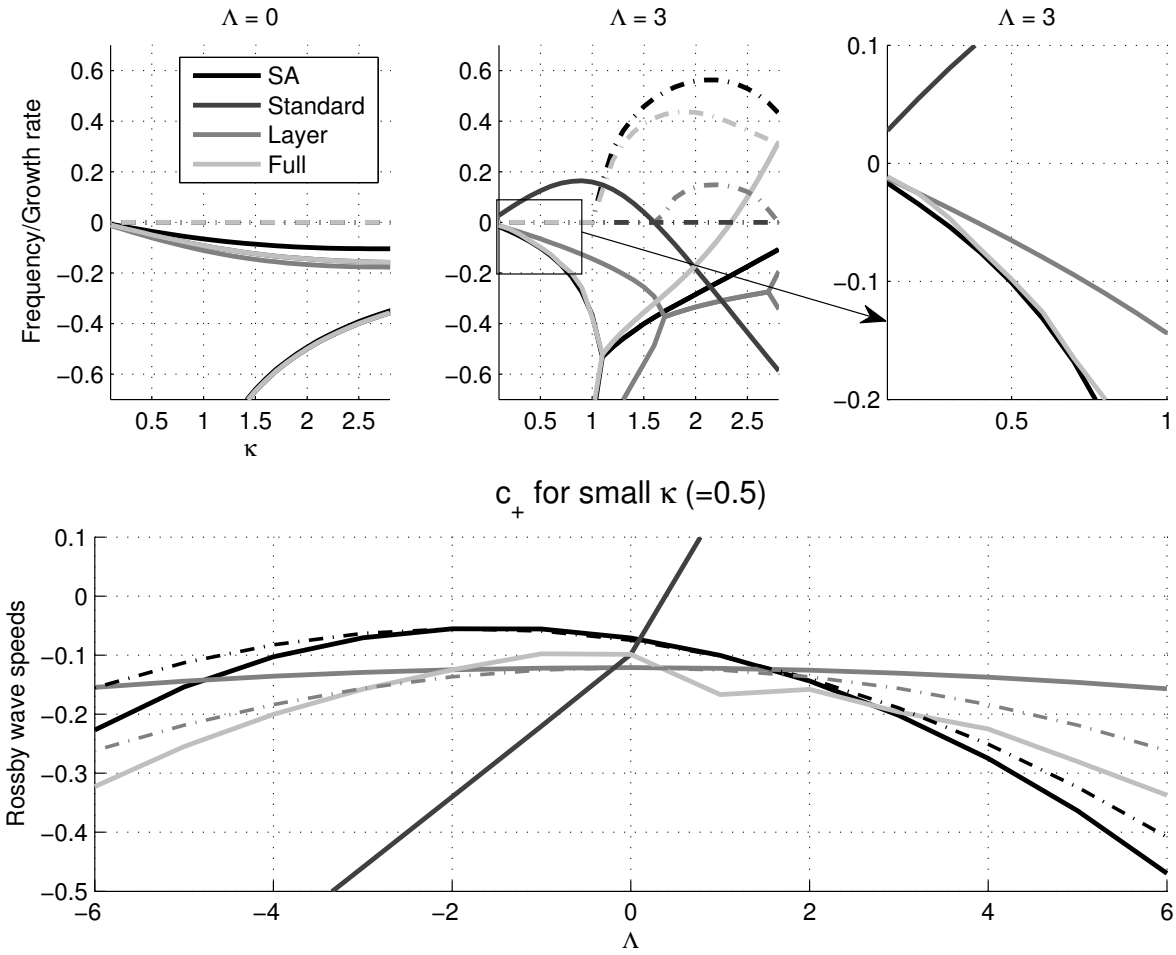

Fig. 4. Top: Comparison of the frequency (solid) and growth rate (dashed) from the two-SA-mode, two-standard-mode, two-layer model, and the full numerical solution for $\Lambda = 0$ (upper left) and 3 (upper middle). The panel on the upper right is a closeup of the stable branch at small wavenumbers for the case with $\Lambda = 3$. Bottom panel: baroclinic Rossby wave speeds for the three truncated models at $\kappa = 0.5$. Dashed lines are the small-κ expansions for the analytic solutions given in (16), up to $O(\kappa^2)$. The full solution (lightest gray line) is the curve on Fig. 3 with $\xi = 0$ but without the absolute value or scaling factor π^2. The discontinuity in the full solution at $\Lambda = 1$ is because the system is stable when $0 < \Lambda < 1$ and changes to an eastward sheared Charney instability as Λ increases. Note that, for the range of Λ plotted, the small-κ expansion for the analytical solution in standard modes overlaps with its numerical solution.

4.2. Exponential stratification

The interaction between surface buoyancy gradients and interior PV gradients in the case of exponential stratification will be investigated with two types of mean flows. We first consider the case with $\xi = 0$. When the interior part of the mean velocity is absent, the corresponding meridional mean PV gradient is $\Pi = 1 - \Lambda$, and therefore the instability will be caused by the interaction between the surface shear flow and the interior PV gradient as in section 4.1. The system with this particular mean flow is investigated with two-SA-mode, two-standard-mode, and two-layer approximations. For the two-layer approximation, the depth of the first layer is taken to be the fractional scale height δ. The top panel of Fig. 5 gives a comparison of frequencies and growth rates among the above three truncations for a few values of Λ. From the dispersion relation, it can be shown that the SA-mode solution and the two-layer approximation agree well with the full solution

for small κ. However, neither the two-layer approximation nor the standard normal mode basis can capture the instability of the system, while SA-mode solutions agree with the full solution, in both frequency and the growth rate, for all scales.

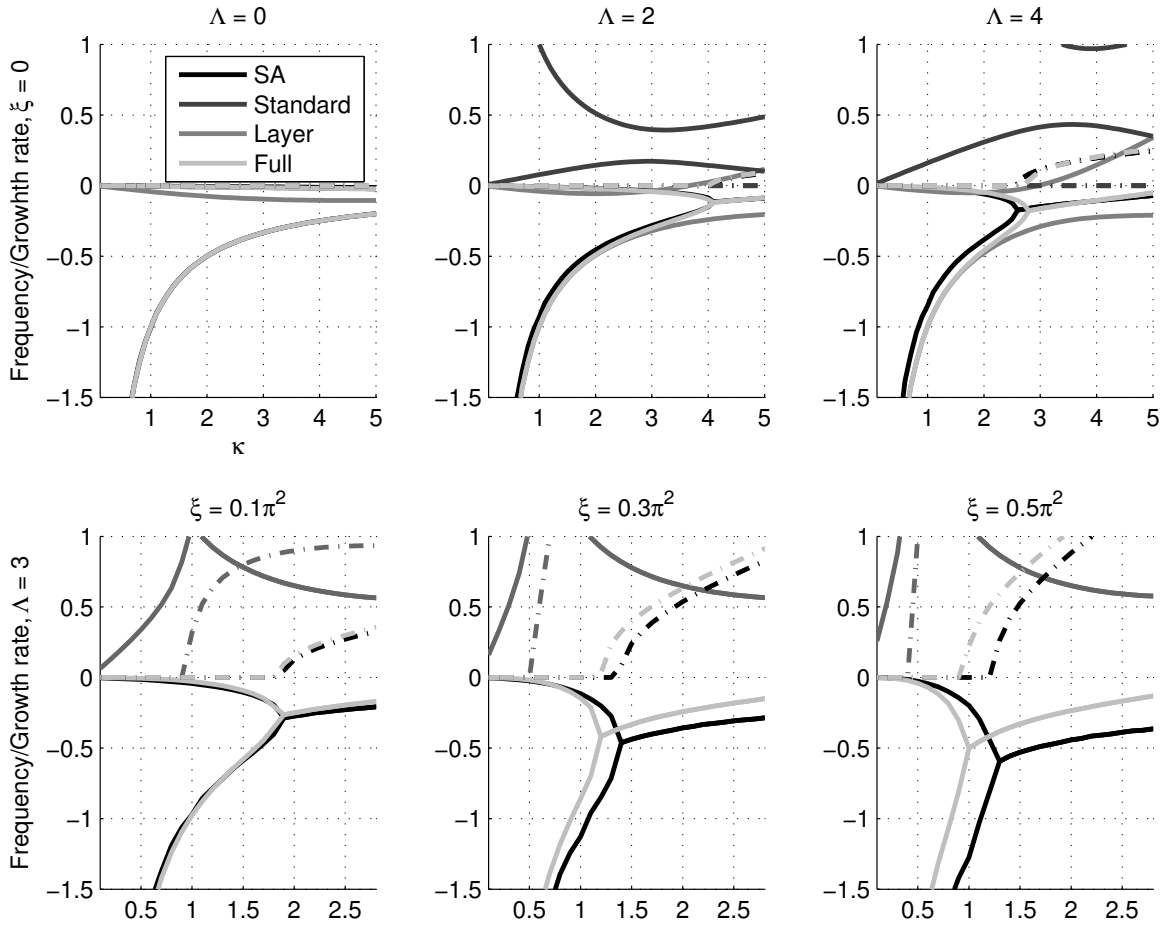

Fig. 5. Top panel: Comparison of frequency (solid) and growth rate (dashed) between the two-SA-mode truncation, two-standard-mode truncation, two-layer model and the full model, for varying Λ with no interior flow ($\xi = 0$). Bottom panel: Comparison of frequency (solid) and growth rate (dashed) between the three-SA-mode truncation, three-standard-mode truncation, and the full model with fixed surface buoyancy gradient $\Lambda = 3$ and varying interior flows, $\xi = (0.1, 0.3, 0.5)\pi^2$.

The second type of mean flow has both surface and interior components, i.e. $U = U^S + U^I$, thus the instability could be of the Charney-type or Phillips-type, or both. For this case, with non-zero interior velocity, three-mode truncations for both the SA and standard mode bases are used (solutions are computed numerically), while the low-resolution layered model is neglected. The bottom panel of Fig. 5 gives the comparison of those solutions with the full solution for different combinations of Λ and ξ. The results show that, comparing to traditional baroclinic modal solution, the SA-mode solution agrees well with the full solution, in both frequency and growth rate.

4.3. The efficiency of the surface-aware modes

A convergence study is preformed to test the efficiency of the SA modal basis when surface buoyancy gradients exist. A comparison is made between two-mode and three-mode truncated solutions in the SA-modal basis for the three cases considered above, namely constant stratification, exponential stratification without interior flow, and exponential stratification with interior flow. Fig. 6 gives the comparison of frequencies

and growth rates of two-mode and three-mode truncations, along with the full numerical solutions, for these three different combinations of mean flows and background stratifications. The results show that SA modes capture the dynamics efficiently with only a few modes. For all cases, the three-SA-mode truncation is sufficient for solving this ocean Charney problem. On the other hand, for the ocean Charney problem discussed here, one should not expect solutions from standard normal modes to agree with the full solutions; since this set of modes cannot form a complete basis for systems with non-vanishing surface buoyancy gradients, uniform convergence is lost if dynamical variables are expanded in these modes.

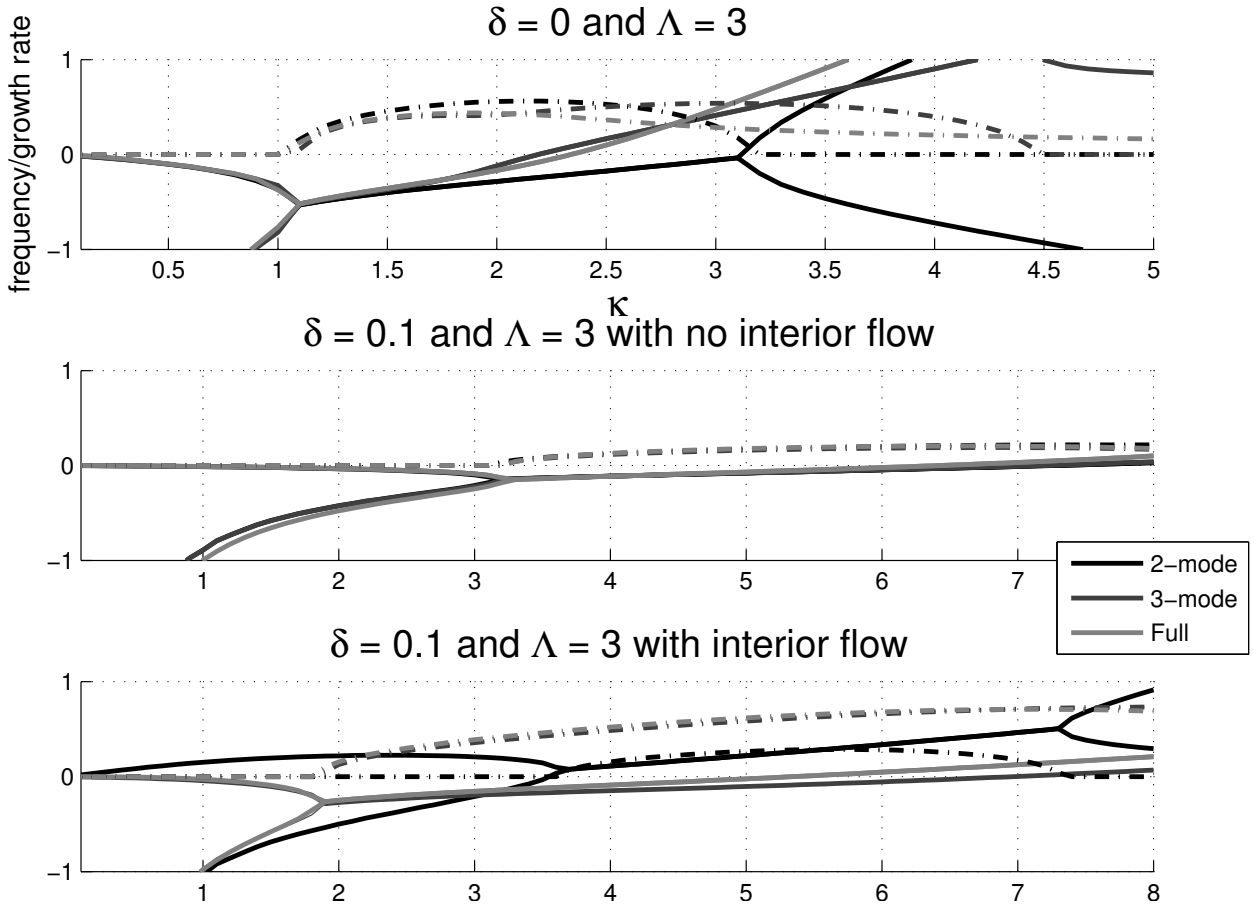

Fig. 6. The efficiency of the surface-aware modes: two-mode and three-mode SA-basis solutions, compared to full numerical solutions, for constant N (Top), exponential N without interior velocity (Middle), and exponential N with interior velocity where $\xi = 0.1\pi^2$ (Bottom).

5. Conclusion and Discussion

Based on our investigation using a simple mean flow configuration to study Rossby wave speeds under the interaction between surface buoyancy gradients and interior PV gradients, we find that in most cases, surface buoyancy gradients yield faster Rossby waves. However, one only arrives at this conclusion when analyzing models that properly represent lateral surface gradients. Since the ocean Charney problem considered here has a non-vanishing boundary condition at the surface, we expect the standard normal mode solutions, which assumes Neumann boundary condition ($\phi_n' = 0$), not to match the full solution well.

Three different truncated models are used to solve the ocean Charney problem, namely a two-layer model, a truncated standard-mode model, and a truncated SA-mode model. Among these three methods, only

the SA-mode model is derived from a non-standard Sturm-Liouville problem with non-vanishing Neumann boundary conditions. Besides taking account of lateral buoyancy gradients, the SA-mode truncated system also provides a systematic way for computing wave speeds. If an n-mode expansion is used, the phase speeds are the eigenvalues of the $n \times n$ matrix formed by eigenmode expansion and projection, as shown in equation (14). Taking advantage of the simplicity of this algorithm, analytical solutions under the two-mode truncation can be written explicitly. This is a fairly simple mathematical model compared to the classic Charney problem (Pedlosky, 1987). Moreover, as shown by comparisons with full solutions obtained by finite difference method, the wave dispersion relation and growth rate can be well described by using only a few modes.

One may notice that there are large discrepancies between the truncated solutions in the standard normal mode basis and the full solutions for all types of mean flows. These discrepancies are caused by the fact that we directly used the mean flow in the wave equations (9) when projecting those equations onto different modes. One could possibly expect a better performance for the solutions if one projected the mean flow onto the traditional baroclinic modes first, then solved the wave equation. However, this approach will eliminate the effects of surface buoyancy gradients on the system since the projected mean flow does not have surface buoyancy gradients. In contrast, since SA modes take into account the information from the surface boundary, it is not surprising that solutions from SA-mode truncation match the full solution. The layer approximation, on the other hand, can be considered as the one which captures the vertically-averaged dynamics of the system. Thus, a layered model works well under linear background stratification because at very large scale, solutions tend to represent the averaged dynamics.

The results suggest that, where lateral surface gradients are present, a conceptual understanding of the wave propagation problems can be obtained by using low-mode truncation in SA-mode basis. Interactions between lateral surface buoyancy gradients and interior background PV gradients exist in many regions in the ocean, and this fact leads to baroclinic instability (Tulloch et al., 2011). Analyzing the OCCA data used in Fig. 1, using local values of f_0, β and N_0 (averaged over the upper 200 m), one finds $|\Lambda| \lesssim 2$ and ξ is $O(10^{-2})$, yielding wave speeds on order twice the long Rossby wave speed, roughly in accord with satellite observations. It may also be worthwhile to apply this simple idea to data from 3D simulations or direct ocean measurements to study surface buoyancy effects on Rossby wave speeds and compare the results with Chelton and Schlax (1996).

Acknowledgments: The authors wish to thank Ross Tulloch for help with analyzing OCCA data; and Ian Grooms, Ed Gerber and Glenn Flierl for helpful discussions. This work was supported by NSF OCE-0962054.

Appendix A: SA-mode construction

Here we review SV13, with a focus on the "ocean limit" (with vanishing lower surface buoyancy gradient) used in the present work. The construction of the SA modes proceeds by simultaneous diagonalization of two quadratic invariants for the system. QG flow conserves

$$E_\kappa = \frac{1}{2}\int_{-1}^{0} (s|\psi'|^2 + \kappa^2|\psi|^2)dz$$
$$Z_\kappa = \frac{1}{2}\int_{-1}^{0} |q|^2 dz$$
$$B_\kappa = \frac{1}{2}|b|^2,$$

which are the energy, potential enstrophy and upper surface buoyancy variance, respectively. In order to force the modes to represent flows with surface buoyancy anomalies, one constructs a "generalized enstrophy"

$$P_\kappa \equiv Z_\kappa + \alpha_+ B_\kappa,$$

where α_+ is an arbitrary nondimensional weight whose role becomes more clear in the eigenvalue problem derived below. To proceed with the derivation, we define a a non-standard generalized PV vector, an inner product, and two operators, as follows. The generalized PV vector is

$$\boldsymbol{Q} = \begin{bmatrix} b \\ q(z) \end{bmatrix} = \begin{bmatrix} \psi'(0) \\ -\kappa^2\psi + (s\psi')' \end{bmatrix} \tag{17}$$

and the inner product is defined as

$$\langle \boldsymbol{Q}_1, \boldsymbol{Q}_2 \rangle = \int_{-1}^{0} q_1^* q_2 \, \mathrm{d}z + b_1^* b_2, \tag{18}$$

where $*$ denotes the complex conjugate. The operators are

$$\mathcal{E}Q = \begin{bmatrix} \psi(0) \\ -\psi(z) \end{bmatrix} \quad \text{and} \quad \mathcal{P}Q = \begin{bmatrix} \alpha_+ b \\ q(z) \end{bmatrix} \tag{19}$$

which are self-adjoint with respect to the inner product defined above. With these definitions, the invariants can be rewritten as

$$E_\kappa = \frac{1}{2}\langle Q, \mathcal{E}Q \rangle \quad \text{and} \quad P_\kappa = \frac{1}{2}\langle Q, \mathcal{P}Q \rangle.$$

Demanding the simultaneous diagonalization of the quadratic forms E_κ and P_κ is equivalent to solving the generalized eigenvalue problem

$$\mathcal{P}\boldsymbol{\xi}_j = \mu_j^2 \mathcal{E}\boldsymbol{\xi}_j$$

where the eigenfunctions $\boldsymbol{\xi}_j$ are analogous in structure to $\boldsymbol{Q}$. Defining modes $\phi_j(z)$ analogous to the streamfunction $\psi(z)$ gives, by the operator definitions (19),

$$\begin{bmatrix} \alpha_+ \xi_j(0) \\ \xi_j(z) \end{bmatrix} = \mu_j^2 \begin{bmatrix} \phi_j(0) \\ -\phi_j(z) \end{bmatrix}. \tag{20}$$

The eigenvectors $\boldsymbol{\xi}_j$ and ϕ_j, as well as the eigenvalues μ_j can be shown to be purely real. The relationships between $\xi_j(z)$, $\xi_j(0)$ and $\phi_j(z)$ are analogous to those between q, b and ψ in (9), respectively, allowing the eigenvalue problem to be written entirely in terms of ϕ_j as

$$(s\phi_j')' - \kappa^2\phi_j = -\mu_j^2\phi_j, \quad \text{with} \quad \phi_j'(0) = \frac{\mu_j^2}{\alpha_+}\phi_j(0), \quad \phi_j'(-1) = 0. \tag{21}$$

Note that in the limit $\alpha_+ \to \infty$, (21) becomes the Sturm-Liouville equation for standard vertical modes (3), which is obvious when μ_j is eliminated in favor of λ_j using the relation $\mu_j^2 = \kappa^2 + \lambda_j^2$. On the other hand, in the limit $\alpha_+ \ll 1$, the "ocean-limit" eigenvalue problem (10) arises. The eigenfunctions are orthogonal in the sense that $\langle \boldsymbol{\xi}_i, \mathcal{E}\boldsymbol{\xi}_j \rangle$ and $\langle \boldsymbol{\xi}_i, \mathcal{P}\boldsymbol{\xi}_j \rangle$ are both zero if and only if $i \neq j$. For our purposes, we choose the normalization

$$\langle \boldsymbol{\xi}_i, \mathcal{E}\boldsymbol{\xi}_j \rangle = \int_{-1}^{0} s\phi_i'\phi_j' + \kappa^2\phi_i\phi_j \, \mathrm{d}z = \mu_j^2\delta_{ij}, \tag{22}$$

which is equivalent to (11) (but differs from that used in SV13). Given PV $q(z)$ and surface buoyancy b, one can construct $\boldsymbol{Q}$ as in (17), and expand in the new modes as

$$\boldsymbol{Q} = \sum_{j=0}^{n} a_j \boldsymbol{\xi}_j,$$

and the coefficients a_j can be recovered using (22), which yields

$$a_j = \frac{1}{\mu_j^2}\left(\int_{-1}^{0} s\phi_j'\psi' + \kappa^2\phi_j\psi \right).$$

Writing the wave equations (9) as a single equation in terms of $\boldsymbol{Q}$ allows one to expand the equation in modes

$$\sum_{j=0}^{n} a_j \left[c\, \boldsymbol{\xi}_j - (\boldsymbol{U} + \boldsymbol{G}) \circ \boldsymbol{\xi}_j \right] = 0, \quad \text{where} \quad \boldsymbol{U} \equiv \begin{bmatrix} U(0) \\ U(z) \end{bmatrix}, \quad \boldsymbol{G} \equiv \begin{bmatrix} -\Lambda \\ \Pi(z) \end{bmatrix}, \tag{23}$$

and $\boldsymbol{A} \circ \boldsymbol{B}$ denotes the Hadamard product, or element-by-element product, of two vectors $\boldsymbol{A}$ and $\boldsymbol{B}$. In order to apply the orthogonality condition, we compute the inner product $\mathcal{E}\boldsymbol{\xi}_i$ and (23) to get

$$\sum_{j} a_j \left[c\, \langle \mathcal{E}\boldsymbol{\xi}_i, \boldsymbol{\xi}_j \rangle - \langle \mathcal{E}\boldsymbol{\xi}_i, (\boldsymbol{U} + \boldsymbol{G}) \circ \boldsymbol{\xi}_j \rangle \right] = 0.$$

By the self-adjoint property of the operator and the orthogonality condition (22), the first inner product on the left is $\mu_j^2 \delta_{ij}$, and the other two terms are

$$\langle \mathcal{E}\boldsymbol{\xi}_i, \boldsymbol{G} \circ \boldsymbol{\xi}_j \rangle = \int_{-1}^{0} -\phi_i \Pi \phi_j \, \mathrm{d}z - \phi_i(0) \Lambda \phi_j(0)$$

and

$$\langle \mathcal{E}\boldsymbol{\xi}_i, \boldsymbol{U} \circ \boldsymbol{\xi}_j \rangle = \int_{-1}^{0} -\phi_i U \left[(s' \phi_j')' - \kappa^2 \phi_j \right] \, \mathrm{d}z + \phi_i(0) U(0) \phi_j'(0).$$

Using the eigenvalue problem (21), the term in braces inside the second integral can be replaced with $-\mu_j^2 \phi_j$. Putting all the results together yields (14) and (15). Note that one could also use the boundary condition in (21) to replace $\phi_j'(0)$ with $(\mu_j^2/\alpha_+)\phi_j(0)$ on the right hand side of the second expression, resulting in the somewhat more succinct form

$$\mathsf{B}_{ij} = \frac{1}{\mu_i^2} \left[\int_{-1}^{0} \left(\mu_j^2 U - \Pi \right) \phi_i \phi_j \, \mathrm{d}z + \left(\frac{\mu_j^2}{\alpha_+} U(0) - \Lambda \right) \phi_i(0) \phi_j(0) \right]. \tag{24}$$

However, this substitution doesn't work with $j > 0$ in the "ocean-limit" used in the present analysis and so the form in (15) is preferred.

Appendix B: Analytical solutions

Expansion in two SA modes

For the case with constant stratification with $U^I = 0$, one can use the expression for $U = U^S$ (5), and the ocean-limit SA modes and eigenvalues in (12) and (13) to compute the matrix B in (15) (a number of elementary but tedious integrations are needed). With these in hand, the matrix on the right hand side of (14) reads

$$\mathsf{B} = \begin{bmatrix} \frac{\Lambda - 1}{\kappa \sinh(2\kappa)} + \frac{\Lambda - 1}{2\kappa^2} - \frac{\Lambda}{\kappa \tanh \kappa} + \frac{\Lambda}{3} & \pi \frac{2\Lambda(\mu_1^2 \kappa \tanh \kappa - 2\kappa^2) + \mu_1^2}{\sqrt{2\alpha_+} \mu_1^4 \kappa \tanh \kappa} \\ \frac{\sqrt{2\alpha_+} \pi (1 - \Lambda)}{2\mu_1^4} & \frac{\Lambda - 1}{\mu_1^4} - \frac{\Lambda}{\pi^2} \end{bmatrix}, \tag{25}$$

where $\mu_1^2 = \kappa^2 + \pi^2/4$ was used to keep the expresion more compact. The eigenvalues can then be solved for explicitly, and the result is

$$c_\pm = \frac{1}{2} \Delta_3 \pm \frac{1}{2} \sqrt{\Delta_1^2 + \Delta_2} \tag{26}$$

where

$$\begin{aligned}
\Delta_1 &= \mathsf{B}_{00} - \mathsf{B}_{11} \\
&= \frac{\Lambda-1}{\kappa\sinh(2\kappa)} + \frac{\Lambda-1}{2\kappa^2} - \frac{\Lambda}{\kappa\tanh\kappa} + \frac{\Lambda}{3} + \frac{1-\Lambda}{\mu_1^4} + \frac{\Lambda}{\pi^2} \\
\Delta_2 &= 4\mathsf{B}_{01}\mathsf{B}_{10} \\
&= 2\pi^2(1-\Lambda)\frac{2\Lambda(\mu_1^2\kappa\tanh\kappa - 2\kappa^2) + \mu_1^2}{\mu_1^8\kappa\tanh\kappa} \\
\Delta_3 &= \mathsf{B}_{00} + \mathsf{B}_{11} \\
&= \frac{\Lambda-1}{\kappa\sinh(2\kappa)} + \frac{\Lambda-1}{2\kappa^2} - \frac{\Lambda}{\kappa\tanh\kappa} + \frac{\Lambda}{3} + \frac{\Lambda-1}{\mu_1^4} - \frac{\Lambda}{\pi^2}
\end{aligned}$$

where B_{ij} are the elements of the matrix in (25). Notice that the phase speeds in equation (26) are independent of the choice of α_+ for the boundary condition of the eigenvalue problem.

Expanding in a Taylor series about $\kappa = 0$ gives

$$\begin{aligned}
c_+ &= -0.08 - 0.02\Lambda + \left(0.009 + 0.01\Lambda - 0.02\Lambda^2\right)\kappa^2 + O(\kappa^4) \\
c_- &= -\frac{1}{\kappa^2} + 0.005(1-\Lambda) + O(\kappa^2).
\end{aligned}$$

Expansion in two standard baroclinic modes

In the limit $\alpha_+ \to \infty$ the modal wave equation (14) becomes a problem for the coefficients of the barotropic and baroclinic modes. In this limit, $\phi_0 = 1$ and $\phi_1 = \sqrt{2}\cos\pi z$, with eigenvalues $\mu_0^2 = \kappa^2$ and $\mu_1 = \kappa^2 + \pi^2$ (since $\lambda_1 = \pi$ in our nondimensionalization). The matrix B can again be computed using (15), and the result is

$$\mathsf{B} = \begin{bmatrix} -\frac{1-\Lambda}{\kappa^2} & \Lambda\frac{\sqrt{2}}{\pi^2}\frac{\kappa^2+\pi^2}{\kappa^2} \\ \Lambda\frac{\sqrt{2}}{\pi^2}\frac{\kappa^2}{\kappa^2+\pi^2} & \frac{\Lambda}{4\pi^2} - \frac{1-\Lambda}{\kappa^2+\pi^2} \end{bmatrix}. \tag{27}$$

This result can be compared to the same analysis in Salmon's textbook (Salmon, 1998). The eigenvalues are

$$\begin{aligned}
c_\pm = -\frac{1-\Lambda}{2\kappa^2} + \frac{(\kappa^2+\pi^2)\frac{\Lambda}{4\pi^2} - (1-\Lambda)}{2(\kappa^2+\pi^2)} \\
\pm \frac{1}{2}\sqrt{\left(-\frac{1-\Lambda}{\kappa^2} - \frac{(\kappa^2+\pi^2)\frac{\Lambda}{4\pi^2} - (1-\Lambda)}{\kappa^2+\pi^2}\right)^2 + \frac{8\Lambda^2}{\pi^4}}
\end{aligned}$$

Expanding about $\kappa = 0$ gives the approximation

$$c_+ = 0.13\Lambda - 0.025 + \left(0.02\frac{\Lambda^2}{1-\Lambda} - 0.01\Lambda + 0.01\right)\kappa^2 + O(\kappa^2) \tag{28}$$

$$c_- = -\frac{1-\Lambda}{\kappa^2} + O(\kappa^2). \tag{29}$$

Two-layer model

The traditional truncation of the Rossby wave equation is discretization into two isopycnal layers. For the case of constant stratification, the layers are taken to have equal depths, $H_1 = H_2$, and for the case of exponential stratification (6), we set $H_1 = \delta$ and $H_2 = H - \delta$. The discrete mean zonal velocities U_1 and U_2 are taken to be vertical averages over the velocity within each layer. The equations for for the streamfunction wave amplitudes ψ_1 and ψ_2 for each layer are (Pedlosky, 1987)

$$(c - U_j)\Big[-\kappa^2\psi_j - F_j(\psi_j - \psi_{3-j})\Big] + \Pi_j\psi_j = 0, \quad j = 1, 2, \tag{30}$$

where, following our nondimensionalization, $F_j = 2(H_1+H_2)/H_j$ (using Pedlosky's notation, $F_j = f_0^2 L^2/(g' H_j)$, where here $N_0^2 = 2g'/H$, and our nondimensionalization length is $L = N_0 H/f_0$). The mean PV gradients are $\Pi_j = 1 - (-1)^j F_j(U_1 - U_2)$. For $U(z) = U^S(z)$, with U^S given by (5), the mean velocities are

$$U_1 = \frac{1}{2}\int_{-1/2}^{0} U(z)\ \mathrm{d}z = \frac{\Lambda}{8} \quad \text{and} \quad U_2 = \frac{1}{2}\int_{-1}^{-1/2} U(z)\ \mathrm{d}z = -\frac{\Lambda}{8} = -U_1.$$

For the case of exponential stratification, integrating U^S in (2) over the two layers gives

$$U_1 = \frac{\Lambda}{6}(\delta^2 - 3\delta + 2) \quad \text{and} \quad U_2 = -\frac{\Lambda}{6}\frac{\delta}{1-\delta}(\delta^2 - 3\delta + 2).$$

The wave speeds in the general case are

$$c = U_2 + \frac{U_s\kappa^2(\kappa^2 + 2F_2) - (2\kappa^2 + F_1 + F_2)}{2\kappa^2(\kappa^2 + F_1 + F_2)} \pm \frac{[(F_1+F_2)^2 + 2U_s\kappa^4(F_1 - F_2) - \kappa^4 U_s^2(4F_1F_2 - \kappa^4)]^{1/2}}{2\kappa^2(\kappa^2 + F_1 + F_2)}$$

where $U_s = U_1 - U_2$. For constant background stratification ($F_1 = F_2$, and $U_s = \Lambda/4$), these are

$$c\pm = -\frac{\kappa^2 + 4}{\kappa^2(\kappa^2 + 8)} \pm \frac{\left[64 - \kappa^4\Lambda^2(4 - \frac{1}{16}\kappa^4)\right]^{1/2}}{2\kappa^2(\kappa^2 + 8)}.$$

A series expansion for small κ yields

$$c_+ = -0.125 + (-0.016\Lambda^2 + 0.016)\kappa^2 + O(\kappa^4) \tag{31}$$

$$c_- = -\frac{1}{\kappa^2} + O(\kappa^2) \tag{32}$$

References

References

Chelton, D. B., Schlax, M. G., 1996. Global observations of oceanic Rossby waves. Science 272, 234–238.

Chelton, D. B., Schlax, M. G., Samelson, R. M., 2011. Global observations of nonlinear mesoscale eddies. Progress in Oceanography 91, 167–216.

Early, J. J., Samelson, R. M., Chelton, D. B., 2011. The evolution and propagation of quasigeostrophic ocean eddies. J. Phys. Oceanogr. 41, 1535–1555.

Flierl, G. R., 1978. Models of vertical structure and the calibration of two-layer models. Dyn. Atmos. Oceans 2, 341–381.

Forget, G., 2010. Mapping ocean observations in a dynamical framework: A 2004-06 ocean atlas. J. Phys. Oceanogr. 40, 1201–1221.

Killworth, P. D., Blundell, J. R., 2003. Long extratropical planetary wave propagation in the presence of slowly varying mean flow and bottom topography. Part I: The local problem. J. Phys. Oceanogr. 33, 784–801.

Killworth, P. D., Chelton, D. B., Szoeke, R. A. D., 1997. The speed of observed and theoretical long extratropical planetary waves. J. Phys. Oceanogr. 29, 1946–1966.

Pedlosky, J., 1987. Geophysical Fluid Dynamics, 2nd Edition. Springer, New York.

Ponte, A. L., Klein, P., 2013. Reconstruction of the upper ocean 3d dynamics from high-resolution sea surface height. Ocean Dynamics 63, 777–791.

Salmon, R., 1998. Lectures on Geophysical Fluid Dynamics. Oxford University Press, New York.

Smith, K. S., 2007. The geography of linear baroclinic instability in Earth's oceans. J. Marine Res. 65, 655–683.

Smith, K. S., Vanneste, J., March 2013. A surface-aware projection basis for quasigeostrophic flow. J. Phys. Oceanogr. 43, 548–562.

Tailleux, R., McWilliams, J. C., 2001. The effect of bottom pressure decoupling on the speed of extratropical, baroclinic Rossby waves. J. Phys. Oceanogr. 31, 1461–1476.

Tulloch, R. T., Marshall, J., Hill, C., Smith, K. S., 2011. Scales, growth rates and spectral fluxes of baroclinic scales, growth rates and spectral fluxes of baroclinic instability in the ocean. J. Phys. Oceanogr. 41, 1057–1076.

Vallis, G. K., 2006. Atmospheric and Oceanic Fluid Dynamics: Fundamentals and Large-Scale Circulation. Cambridge University Press, Cambridge, U.K.

Wang, J., Flierl, G. R., LaCasce, J. H., McClean, J. L., Mahadevan, A., 2013. Reconstructing the ocean's interior from surface data. J. Phys. Oceanogr. 43, 1611–1626.

Xu, Y., Fu, L., 2011. Global varibility of the wavenumber spectrum of oceanic mesoscale turbulence. J. Phys. Oceanogr. 41, 802–809.